

Fig. 2. Key waveforms in: (a) DCMa and (b) DCMb operation of boost inductor.

where the peak inductor current is

$$i_{LBpk} = \frac{v_{in}^{rec} - \frac{N_1}{N_P} V_B}{L_B f_s} \cdot D. \quad (3)$$

From the flux balance of the boost inductor

$$\left( v_{in}^{rec} - \frac{N_1}{N_P} \cdot V_B \right) \cdot D = \left[ \left( 1 + \frac{N_2}{N_R} \right) \cdot V_B - v_{in}^{rec} \right] \cdot D_{rLB} \quad (4)$$

it follows that

$$D + D_{rLB} = \frac{1 - \frac{N_1}{N_P} + \frac{N_2}{N_R}}{1 + \frac{N_2}{N_R} - \frac{v_{in}^{rec}}{V_B}} \cdot D. \quad (5)$$

Substituting (3) and (5) into (2), the average boost inductor current in DCMa is obtained as

$$i_{LBav}^{DCMa} = \frac{V_B D^2}{2L_B f_s} \cdot \frac{A_1 + A_2 \frac{v_{in}^{rec}}{V_B}}{1 + \frac{N_2}{N_R} - \frac{v_{in}^{rec}}{V_B}} \quad (6)$$

where

$$A_2 = 1 - \frac{N_1}{N_P} + \frac{N_2}{N_R}$$

and

$$A_1 = -\frac{N_1}{N_P} A_2. \quad (7)$$

In DCMb, the average boost inductor current is determined as

$$i_{LBav}^{DCMb} = \frac{D + D_{rXF}}{2} \cdot i_{LBpk} + \frac{D_{rXF} + \Delta D_{rLB}}{2} \cdot i_{LB rXF} \quad (8)$$

where

$$D_{rXF} = \frac{N_R}{N_P} \cdot D \quad (9)$$

is the transformer-reset cycle,  $i_{LBpk}$  is the peak inductor current defined in (3),  $i_{LB rXF}$  is the boost inductor current at the moment the transformer core reset is completed, i.e.,

$$i_{LB rXF} = \frac{V_B - v_{in}^{rec}}{L_B f_s} \cdot \Delta D_{rLB} \quad (10)$$

and  $\Delta D_{rLB}$  represents the additional reset interval of  $L_B$  after the reset of the transformer is completed.  $\Delta D_{rLB}$  can be obtained from the flux balance of  $L_B$

$$\left( v_{in}^{rec} - \frac{N_1}{N_P} \cdot V_B \right) \cdot D = \left[ \left( 1 + \frac{N_2}{N_R} \right) \cdot V_B - v_{in}^{rec} \right] \cdot \frac{N_R}{N_P} \cdot D + (V_B - v_{in}^{rec}) \cdot \Delta D_{rLB}. \quad (11)$$

From (11), it follows that

$$\Delta D_{rLB} = \frac{\left( 1 + \frac{N_R}{N_P} \right) \cdot \frac{v_{in}^{rec}}{V_B} - \frac{N_R + N_1 + N_2}{N_P}}{1 - \frac{v_{in}^{rec}}{V_B}} \cdot D. \quad (12)$$

Substituting (3), (9), (10), and (12) into (8), the average boost inductor current in DCMb is obtained as

$$i_{LBav}^{DCMb} = \frac{V_B D^2}{2L_B f_s} \cdot \frac{B_1 + B_2 \frac{v_{in}^{rec}}{V_B}}{1 - \frac{v_{in}^{rec}}{V_B}} \quad (13)$$

where

$$B_1 = \left( \frac{N_1 + N_2}{N_P} \right)^2 - \frac{N_1}{N_P} + \frac{N_2 N_R}{N_P^2} \quad (14)$$

and

$$B_2 = 1 - \frac{N_1}{N_P} - \frac{N_2}{N_P} \cdot \left( 2 + \frac{N_R}{N_P} \right). \quad (15)$$

The boundary condition between DCMa and DCMb operations can be found from (12). The condition for operation of  $L_B$  in DCMb is  $\Delta D_{rL_B} > 0$ , i.e.,

$$v_{in}^{rec} > \frac{N_R + N_1 + N_2}{N_R + N_P} \cdot V_B \quad (16)$$

whereas the boundary angle between DCMa and DCMb is defined as

$$\theta_{ab} = a \sin \left( \frac{N_R + N_1 + N_2}{N_R + N_P} \cdot \frac{V_B}{V_{im}} \right). \quad (17)$$

The operation modes of the DCM boost inductor are summarized in Fig. 3. A typical line current waveform is also shown in Fig. 3. The zero-crossing angle (dead angle)  $\theta_d$  is defined as

$$\theta_d = a \sin \left( \frac{N_1}{N_P} \cdot \frac{V_B}{V_{im}} \right). \quad (18)$$

### B. Design

Since the energy-storage capacitor voltage  $V_B$  in a S4ICS is not regulated, it varies with the input line. To minimize the cost, it is desirable to keep  $V_B$  below 400 V so that a capacitor with a rated voltage of 450 V can be safely used. Therefore, the design goal is to keep energy-storage-capacitor voltage  $V_B$  between a maximum value,  $V_{Bmax}$  (e.g.,  $V_{Bmax} = 400$  V), and a minimum value,  $V_{Bmin}$  [determined from the condition to keep  $L_B$  in DCM, see (26)], and to satisfy the line-current harmonic standards such as, for example, IEC 1000-3-2 [12]. The design parameters are  $L_B$ ,  $L_F$ ,  $N_P$ ,  $N_R$ ,  $N_S$ ,  $N_1$ , and  $N_2$ . Voltage  $V_B$  can be obtained from the input-output power balance

$$\frac{2}{\pi} \int_{\theta_d}^{\theta_{ab}} i_{L_{Bav}}^{DCMa} v_{in}^{rec} d\theta + \frac{2}{\pi} \int_{\theta_{ab}}^{\pi-\theta_{ab}} i_{L_{Bav}}^{DCMb} v_{in}^{rec} d\theta = \frac{V_o I_o}{\eta} \quad (19)$$

where  $\eta$  is the assumed efficiency of the converter.

Voltage  $V_B$  reaches  $V_{Bmax}$  at high line when forward inductor  $L_F$  starts to operate at its DCM-CCM boundary, which occurs at some output current  $I_{oDCH} \leq I_{o max}$ . In fact, when  $L_F$  operates in CCM, the bulk-capacitor voltage increases with decreasing output current; however, when  $L_F$  enters DCM, voltage  $V_B$  does not depend on the output current any more, as explained in [3]. To achieve higher efficiency, it is desirable the DCM-CCM boundary of  $L_F$  to occur at a smaller output current. Output current  $I_{oDCH}$  is determined as

$$I_{oDCH} = \frac{(V_o + V_F) \cdot (1 - D_{min})}{2L_F f_S} \quad (20)$$

where the minimum duty cycle,  $D_{min}$ , is obtained from the flux balance of  $L_F$  as

$$D_{min} = \frac{N_P}{N_S} \cdot \frac{V_o + V_F}{V_{Bmax}}. \quad (21)$$

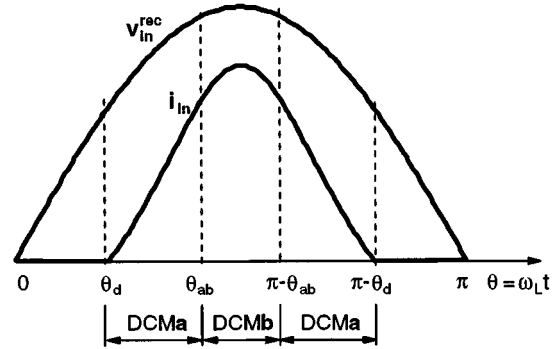


Fig. 3. Operation modes of DCM boost inductor.

Substituting (1), (6), (7), (13)–(15), (20), and (21) into (19) at high line ( $v_{in} = V_{imH} \sin(\omega_L t)$ ) when  $V_B = V_{Bmax}$ , the ratio of the boost and forward inductances can be obtained as

$$\frac{L_B}{L_F} = \frac{2\eta_H}{\pi} \cdot \frac{V_{imH}}{1 - \frac{N_P}{N_S} \cdot \frac{V_o + V_F}{V_{Bmax}}} \cdot \left( \frac{N_P}{N_S} \right)^2 \cdot \left( 1 + \frac{V_F}{V_o} \right) \cdot K_H \quad (22)$$

where  $\eta_H$  is the assumed efficiency of the converter at high line and

$$K_H = \int_{\theta_{dH}}^{\theta_{abH}} A_2 \frac{\frac{V_{imH}}{V_{Bmax}} \sin(\theta) - \frac{N_1}{N_P}}{1 + \frac{N_2}{N_R} - \frac{V_{imH}}{V_{Bmax}} \sin(\theta)} \cdot \sin(\theta) d\theta + \int_{\theta_{abH}}^{\pi/2} \left[ \frac{B_1 \sin(\theta) + B_2 \frac{V_{imH}}{V_{Bmax}} \sin^2(\theta)}{1 - \frac{V_{imH}}{V_{Bmax}} \sin(\theta)} \right] d\theta. \quad (23)$$

In (23),  $\theta_{dH}$  is the zero-crossing angle, defined in (18), and  $\theta_{abH}$  is the DCMa–DCMb boundary angle, defined in (17), at high line ( $V_{im} = V_{imH}$ ) and  $V_B = V_{Bmax}$ .

Voltage  $V_B = V_{Bmin}$  at low line and full load when forward inductor  $L_F$  operates in CCM.  $V_{Bmin}$  is determined from the condition to keep  $L_B$  in DCM, as shown in (29).

Writing  $I_o = I_{o max}$  in (19) and substituting (1), (6), (7), and (13)–(15) into (19) at low line ( $v_{in} = V_{imL} \sin(\omega_L t)$ ) when  $V_B = V_{Bmin}$ , the product of the boost inductance and switching frequency can be obtained as

$$L_B f_S = \frac{\eta_L}{\pi} \cdot \frac{V_{imL}}{I_{o max}} \cdot \left( \frac{N_P}{N_S} \right)^2 \cdot \frac{(V_o + V_F)^2}{V_o} \cdot K_L \quad (24)$$

where  $\eta_L$  is the assumed efficiency of the converter at low line, and  $K_L$  is determined by the same expression as (23), by replacing  $V_{imH}$ ,  $V_{Bmax}$ ,  $\theta_{dH}$ , and  $\theta_{abH}$  with  $V_{imL}$ ,  $V_{Bmin}$ ,  $\theta_{dL}$ , and  $\theta_{abL}$ , respectively.

Using (22) and (24), for selected values of  $N_P$ ,  $N_R$ ,  $N_S$ ,  $N_1$ , and  $N_2$ , and selected switching frequency  $f_S$ , the inductances  $L_B$  and  $L_F$  will be determined. The values of  $N_P$ ,  $N_R$ , and  $N_S$  should be selected as for the conventional dc–dc forward converter. Finally,  $N_1$  and  $N_2$  should be selected according to

the following considerations. To keep the operation of  $L_B$  in DCM, the condition

$$D + D_{rXF} + \Delta D_{rLB} \leq 1 \quad (25)$$

should be satisfied (see Fig. 2). Substituting (9) and (12) into (25) and using the flux balance of  $L_F$ , it follows that

$$V_B \geq V_{im} + \left( \frac{N_P}{N_S} - \frac{N_1 + N_2}{N_S} \right) \cdot (V_o + V_F). \quad (26)$$

Applying (26) at high line, the minimum value of  $N_1 + N_2$  can be obtained as

$$\frac{N_1 + N_2}{N_P} \geq 1 - \frac{V_{B\max} - V_{imH}}{\left( \frac{N_P}{N_S} \right) \cdot (V_o + V_F)}. \quad (27)$$

The maximum value of  $N_1 + N_2$  is determined from the requirement for proper operation of the circuit during on time of the switch [6]

$$\frac{N_1 + N_2}{N_P} < 1. \quad (28)$$

Applying (26) at low line, the minimum value of voltage  $V_B$  can be calculated as

$$V_{B\min} \geq V_{imL} + \left( \frac{N_P}{N_S} - \frac{N_1 + N_2}{N_S} \right) \cdot (V_o + V_F). \quad (29)$$

To optimize the performance,  $V_{B\min}$  should be as small as possible. It follows from (29) that smaller  $V_{B\min}$  will be achieved with larger  $N_1 + N_2$ . Therefore,  $N_1 + N_2$  should be selected close to its maximum possible value, i.e.,  $N_1 + N_2$  should be equal to the number of primary turns reduced by one or two turns.

After selecting the sum  $N_1 + N_2$ , the value of  $N_1$  should be determined from the tradeoff between direct energy transfer and, therefore, higher efficiency (larger  $N_1$ ), and zero-crossing distortion of the line current, associated with lower power factor and higher total harmonic distortion (THD) (smaller  $N_1$ ). In fact,  $N_1$  should be selected as large as possible to achieve higher efficiency and still to satisfy the line-current harmonic standards such as, for example, IEC 1000-3-2 [12].

### C. Design Example

The design procedure is illustrated on the example of a 5-V/20-A universal line-voltage range (90–264 V<sub>rms</sub>) S4ICS forward converter with reset winding. Maximum bulk-capacitor voltage  $V_{B\max} = 400$  V was specified.

First,  $N_S = 3$  is selected, which is a typical number of secondary turns in computer power supplies with multiple outputs. The number of primary turns  $N_P$  should be as large as possible to maximize efficiency. However, the maximum  $N_P$  is limited by the maximum duty cycle,  $D_{\max} < 0.5$ , at low line. According to the considerations in the previous section,  $N_1 + N_2 = N_P - 2$  is selected, which, from (29), yields  $V_{B\min} = 131$  V ( $V_F = 0.55$  V). From the flux balance of  $L_F$ , it follows that a possible range of  $N_P$  is  $N_P = 30$ – $34$ ,

which corresponds to  $D_{\max} = 0.42$ – $0.48$ . To minimize the voltage stress on the switch,  $N_R = N_P$  is selected. For the selected values, design curves are presented in Fig. 4. As can be seen from Fig. 4(a) and (b), with increasing  $N_1$ , product  $L_B f_S$  is decreasing and product  $L_F f_S$  is increasing. (Equivalently, with increasing  $L_F f_S$ , the ratio  $I_{oDCH}/I_{o\max}$ , which represents the DCM-CCM boundary of  $L_F$  at high line when  $V_B$  reaches  $V_{B\max}$ , is decreasing, i.e.,  $L_F$  operates in CCM in a wider range of the output current.) Also, with increasing  $N_1$ , the THD of the line current is increasing and the power factor (PF) is decreasing as shown in Fig. 4(c). Fig. 4(c) also shows the third harmonic of the line current (which is usually the most critical harmonic) related to the IEC 1000-3-2 Class-D limit [12]. The curves in Fig. 4(c) are obtained at nominal low line,  $V_i = 100$  V<sub>rms</sub>, and full load. (The limits for  $V_i = 100$  V<sub>rms</sub> are calculated by multiplying the nominal high line,  $V_i = 230$  V<sub>rms</sub>, limits with  $230/100 = 2.3$ .) The corresponding curves for  $V_i = 230$  V<sub>rms</sub> are almost identical to the curves in Fig. 4(c). Line current waveforms for three different values of  $N_1$  and  $N_P = 32$  (as example), at  $V_i = 100$  V<sub>rms</sub> and 230 V<sub>rms</sub> are given in Fig. 5. As can be seen, the line current has almost identical waveforms at low and high lines. In Fig. 5, the IEC 1000-3-2 Class-D envelopes as well as the ideal, sinusoidal line current waveform are also shown. To keep the third harmonic below, e.g., 80% of the IEC 1000-3-2 Class-D limit, it follows from Fig. 4(c) that  $N_1$  should be smaller than 22, 21, and 20 for  $N_P = 34$ , 32, and 30, respectively. A good design compromise is to select  $N_P = 32$ ,  $N_1 = 20$ , and  $N_2 = 10$ . Then, from Fig. 4(a) and (b),  $L_B f_S = 2.7$  HHz and  $L_F f_S = 0.161$  HHz (e.g., selecting  $f_S = 75$  kHz yields  $L_B = 36$   $\mu$ H and  $L_F = 2.1$   $\mu$ H), which results in THD = 60.1%,  $I_{3h}/I_{3hLim} \approx 74.5\%$ , and PF = 0.857 at both nominal low and high lines.

## III. CCM OPERATION OF BOOST INDUCTOR

### A. Analysis

For CCM operation of the boost inductance, it is necessary to have a substantial inductance connected in series with winding  $N_1$  and/or winding  $N_2$ . The additional inductance can be the leakage inductance of the winding (achieved by an appropriate structure of the transformer) and/or an external inductance. This inductance provides the variable duty cycle for  $L_B$  to operate in CCM. Key waveforms which illustrate principle of operation are given in Fig. 6 for the case of  $L_1 \gg L_2$ . After switch SW is turned on at the beginning of a switching cycle, boost-inductor current  $i_{LB}$  starts to commute from winding  $N_2$  (current  $i_2$ ) to winding  $N_1$  (current  $i_1$ ). Because of inductance  $L_1$ , the slope of current  $i_1$  is limited

$$\frac{di_1}{dt} = \frac{\left( 1 - \frac{N_1 + N_2}{N_P} \right) V_B}{L_1} \quad (30)$$

and the commutation cycle  $\Delta D$  is not negligible compared to duty cycle  $D$ . As can be seen from Fig. 6, because of  $\Delta D$ , the effective duty cycle “seen” by the boost inductor is reduced

$$D_{LB} = D - \Delta D. \quad (31)$$

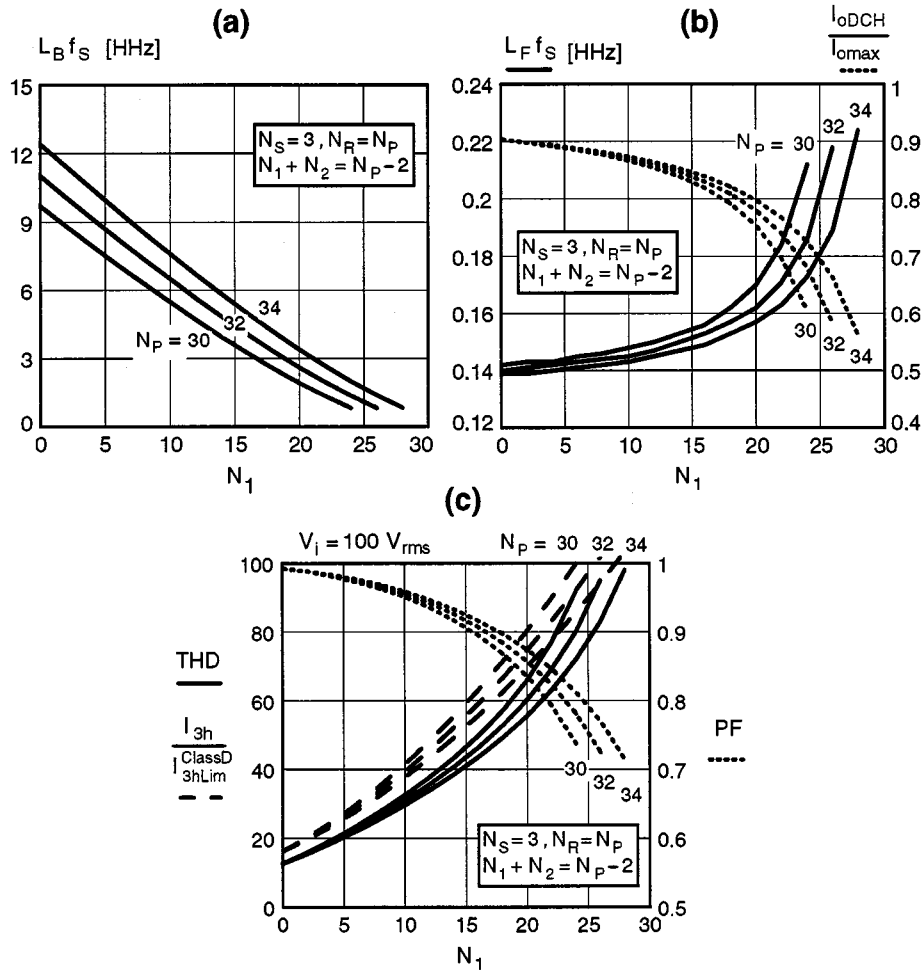


Fig. 4 Design curves for DCM operation of boost inductor ( $V_o = 5$  V,  $I_{o,max} = 20$  A).

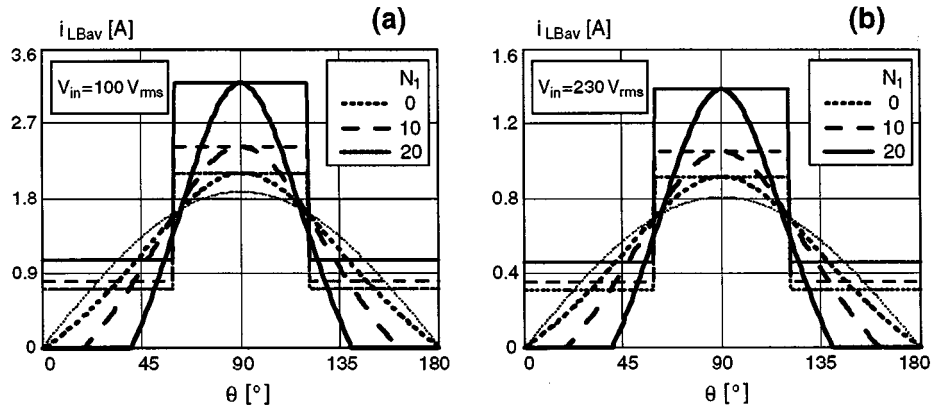


Fig. 5. Line current waveforms in DCM operation of boost inductor ( $V_o = 5$  V,  $I_o = 20$  A,  $N_S = 3$ ,  $N_P = N_R = 32$ ,  $N_1 + N_2 = 30$ ).

Commutation cycle  $\Delta D$  can be obtained from the flux balance of  $L_B$ , i.e.,

$$\frac{v_{in}^{rec} - \frac{N_1}{N_P} \cdot V_B}{1 + \frac{L_1}{L_B}} \cdot (D - \Delta D)$$

$$= \left[ \left( 1 + \frac{N_2}{N_R} \right) \cdot V_B - v_{in}^{rec} \right] \cdot \frac{N_R}{N_P} \cdot D + (V_B - v_{in}^{rec}) \cdot \left( 1 - D - \frac{N_R}{N_P} D \right) + \left( V_B \left( 1 - \frac{N_2}{N_P} \right) - v_{in}^{rec} \right) \cdot \Delta D. \quad (32)$$

After a few simple algebraic operations,  $\Delta D$  is obtained as

$$\Delta D = D - \frac{\left(1 + \frac{L_1}{L_B}\right) \cdot \left(1 - \frac{v_{in}^{rec}}{V_B}\right)}{1 - \frac{N_1 + N_2}{N_P} + \frac{L_1}{L_B} \cdot \left(1 - \frac{N_2}{N_P} - \frac{v_{in}^{rec}}{V_B}\right)}. \quad (33)$$

As can be seen from (33), the effective duty cycle “seen” by the boost inductor is

$$D_{LB} = D - \Delta D \sim 1 - \frac{v_{in}^{rec}}{V_B} \quad (34)$$

which corresponds to the conventional CCM boost ICS. Note that  $D_{LB}$  is approximately equal to  $(1 - v_{in}^{rec}/V_B)$  at  $N_1 = 0$ ,  $N_2 = 0$ , and  $L_1 \ll L_B$ .

To achieve CCM operation of  $L_B$ ,  $\Delta D$  must be greater than or equal to zero. From (33), it follows that

$$v_{in}^{rec} \geq \left(1 - \frac{1 - \frac{N_1}{N_P} - \left(1 + \frac{L_1}{L_B}\right) \cdot \frac{N_2}{N_P} \cdot D}{1 + \frac{L_1}{L_B} \cdot (1 - D)}\right) \cdot V_B. \quad (35)$$

Therefore, the boundary angle between DCM and CCM operations of  $L_B$  is defined as

$$\theta_{bc} = a \sin \left[ \left(1 - \frac{1 - \frac{N_1}{N_P} - \left(1 + \frac{L_1}{L_B}\right) \cdot \frac{N_2}{N_P} \cdot D}{1 + \frac{L_1}{L_B} \cdot (1 - D)}\right) \cdot \frac{V_B}{V_{im}} \right]. \quad (36)$$

In CCM, the average boost inductor current is determined as (see Fig. 6)

$$i_{LB_{av}}^{CCM} = I_0 + \frac{D + D_{rXF} - \Delta D}{2} \cdot \Delta I_1 + \frac{1 - D}{2} \cdot (\Delta I_1 - \Delta I_2) + \frac{1 - D - D_{rXF} + \Delta D}{2} \cdot \Delta I_3 \quad (37)$$

where

$$I_0 = \frac{\left(1 - \frac{N_1 + N_2}{N_P}\right) \cdot V_B}{L_1 f_S} \cdot \Delta D \quad (38)$$

$$\Delta I_1 = \frac{v_{in}^{rec} - \frac{N_1}{N_P} \cdot V_B}{(L_B + L_1) f_S} \cdot (D - \Delta D) \quad (39)$$

$$\Delta I_2 = \frac{\left(1 + \frac{N_2}{N_R}\right) \cdot V_B - v_{in}^{rec}}{L_B f_S} \cdot D_{rXF} \quad (40)$$

$$\Delta I_3 = \frac{\left(1 - \frac{N_2}{N_P}\right) \cdot V_B - v_{in}^{rec}}{L_B f_S} \cdot \Delta D. \quad (41)$$

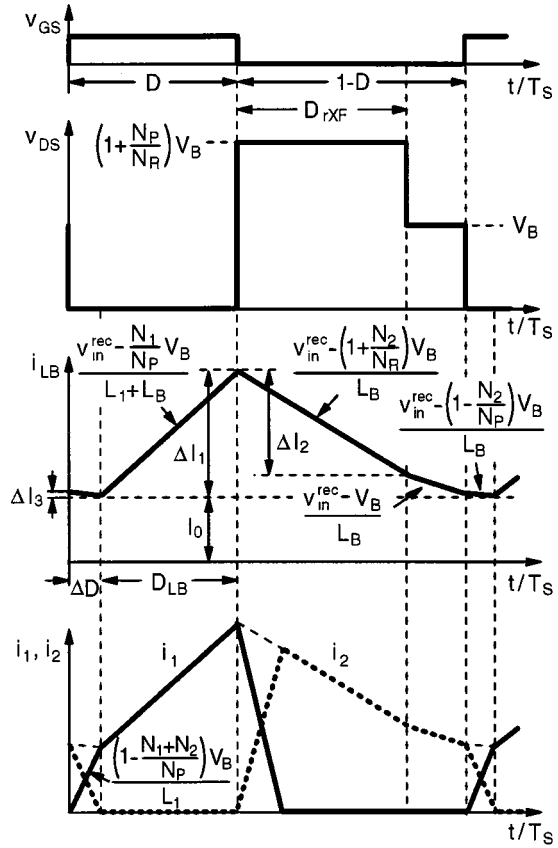


Fig. 6. Key waveforms in CCM operation of boost inductor.

Substituting (9), (33), and (38)–(41) into (37), after a number of simple algebraic operations, the average boost inductor current in CCM is obtained as

$$i_{LB_{av}}^{CCM} = \frac{V_B}{L_1 f_S} \left(1 - \frac{N_1 + N_2}{N_P}\right) \cdot \left[ D - \frac{\left(1 + \frac{L_1}{L_B}\right) \cdot \left(1 - \frac{v_{in}^{rec}}{V_B}\right)}{C_2 - \frac{L_1}{L_B} \frac{v_{in}^{rec}}{V_B}} \right] + \frac{V_B}{2L_B f_S} \left[ C_0(D) + \frac{\left(1 - \frac{v_{in}^{rec}}{V_B}\right) \cdot \left(C_1 + \frac{v_{in}^{rec}}{V_B}\right)}{C_2 - \frac{L_1}{L_B} \frac{v_{in}^{rec}}{V_B}} \right] \quad (42)$$

where

$$C_0(D) = -2D \left(1 - \frac{N_R + N_P}{2N_P} D\right) \cdot \frac{N_2}{N_P} \quad (43)$$

$$C_1 = -\frac{N_1}{N_P} + \frac{N_2}{N_P} \left(1 + \frac{L_1}{L_B}\right) \quad (44)$$

and

$$C_2 = 1 - \frac{N_1 + N_2}{N_P} + \frac{L_1}{L_B} \left(1 - \frac{N_2}{N_P}\right). \quad (45)$$

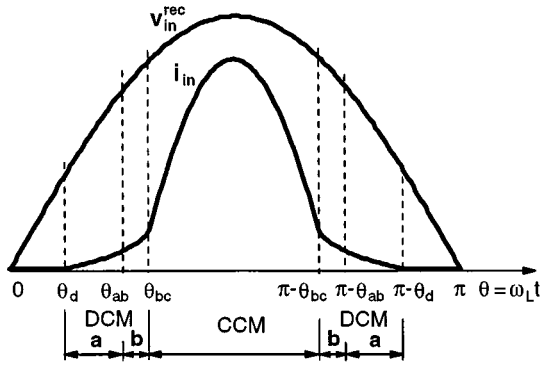


Fig. 7. Operation modes of CCM boost inductor.

For further calculations, it is convenient to rewrite (42) in the following form:

$$i_{L_{Bav}}^{CCM} = \frac{K_{L1}^{CCM}}{L_1 f_s} + \frac{K_{LB}^{CCM}}{L_B f_s}. \quad (46)$$

During a half of a line cycle, before entering CCM, the boost inductor operates in two DCM's, as described in Section II. Following the same derivation procedure as in Section II, the average boost inductor current in the two DCM's is obtained as

$$i_{L_{Bav}}^{DCMa} = \frac{V_B D^2}{2L_B f_s} \cdot \frac{A_1 + A_2 \frac{v_{in}^{rec}}{V_B} + \frac{L_1}{L_B} \left( A_3 + A_4 \frac{v_{in}^{rec}}{V_B} - \left( \frac{v_{in}^{rec}}{V_B} \right)^2 \right)}{\left( 1 + \frac{L_1}{L_B} \right)^2 \left( 1 + \frac{N_2}{N_R} - \frac{v_{in}^{rec}}{V_B} \right)} \quad (47)$$

where  $A_1$  and  $A_2$  are defined in (7)

$$A_3 = - \left( 1 + \frac{N_2}{N_R} \right) \frac{N_1}{N_P}$$

and

$$A_4 = 1 + \frac{N_1}{N_P} + \frac{N_2}{N_R} \quad (48)$$

whereas

$$i_{L_{Bav}}^{DCMb} = \frac{V_B D^2}{2L_B f_s} \cdot \frac{B_1 + B_2 \frac{v_{in}^{rec}}{V_B} + \frac{L_1}{L_B} \left( B_3 + B_4 \frac{v_{in}^{rec}}{V_B} - \left( \frac{v_{in}^{rec}}{V_B} \right)^2 \right)}{\left( 1 + \frac{L_1}{L_B} \right)^2 \left( 1 - \frac{v_{in}^{rec}}{V_B} \right)} \quad (49)$$

where  $B_1$  and  $B_2$  are defined in (14) and (15), respectively,

$$B_3 = \frac{N_1}{N_P} \left( \frac{2N_2}{N_P} - 1 \right) + \frac{(N_2 + N_R)N_2}{N_P^2} \left( 2 + \frac{L_1}{L_B} \right) \quad (50)$$

and

$$B_4 = 1 + \frac{N_1 - 2N_2}{N_P} - \frac{N_2 N_R}{N_P^2} \left( 2 + \frac{L_1}{L_B} \right). \quad (51)$$

Again, for further calculations it is convenient to rewrite (47) and (49) as

$$i_{L_{Bav}}^{DCMa} = \frac{K_{LB}^{DCMa}}{L_B f_s}$$

and

$$i_{L_{Bav}}^{DCMb} = \frac{K_{LB}^{DCMb}}{L_B f_s}. \quad (52)$$

Finally, the boundary angle between DCMa and DCMb is defined as

$$\theta_{ab} = a \sin \left( \frac{N_1 + (N_2 + N_R) \left( 1 + \frac{L_1}{L_B} \right)}{N_P + N_R \left( 1 + \frac{L_1}{L_B} \right)} \cdot \frac{V_B}{V_{im}} \right). \quad (53)$$

The operation modes of the CCM boost inductor are summarized in Fig. 7. A typical line current waveform is also shown in Fig. 7. The zero-crossing angle  $\theta_d$  is defined in (18).

## B. Design

The design goal is, as already described in Section II, to keep energy-storage-capacitor voltage  $V_B$  between a maximum value,  $V_{Bmax}$ , and a minimum value,  $V_{Bmin}$ , and to satisfy the line-current harmonic standards such as, for example, IEC 1000-3-2 [12]. The design parameters are  $L_B$ ,  $L_1$ ,  $L_F$ ,  $N_P$ ,  $N_R$ ,  $N_S$ ,  $N_1$ , and  $N_2$ .

Voltage  $V_B$  can be obtained from the input–output power balance. Using (46) and (52), the input–output power balance can be written as

$$\begin{aligned} \frac{1}{L_B f_s} \cdot \left( \frac{2}{\pi} \int_{\theta_d}^{\theta_{ab}} K_{LB}^{DCMa} v_{in}^{rec} d\theta + \frac{2}{\pi} \int_{\theta_{ab}}^{\theta_{bc}} K_{LB}^{DCMb} v_{in}^{rec} d\theta \right. \\ \left. + \frac{2}{\pi} \int_{\theta_{bc}}^{\pi/2} K_{LB}^{CCM} v_{in}^{rec} d\theta \right) \\ + \frac{1}{L_1 f_s} \cdot \left( \frac{2}{\pi} \int_{\theta_{bc}}^{\pi/2} K_{L1}^{CCM} v_{in}^{rec} d\theta \right) \\ = \frac{V_o I_o}{\eta} \quad (54) \end{aligned}$$

where  $\eta$  is the assumed efficiency of the converter.

Similarly to the S<sup>4</sup>ICS with DCM operation of  $L_B$ , voltage  $V_B = V_{Bmax}$  at high line when  $L_F$  operates at the DCM-CCM boundary at some output current  $I_{oDCH} \leq I_{o,max}$ . Substituting (1), (7), (14), (15), (42)–(45), and (47)–(51) into (54) at high line ( $v_{in} = V_{imH} \sin(\omega_L t)$ ) and  $V_B = V_{Bmax}$ , the input–output power balance yields

$$\frac{K_{LBH}}{L_B f_s} + \frac{K_{L1H}}{L_1 f_s} = \frac{V_o I_{oDCH}}{\eta_H} \quad (55)$$

where  $K_{LBH}$  and  $K_{L1H}$  represent the expressions in the first and second parenthesis on the left side of (54);  $I_{oDCH}$  is defined in (20).

Voltage  $V_B = V_{Bmin}$  at low line and full load when  $L_F$  operates in CCM.  $V_{Bmin}$  should be selected to be slightly larger than the amplitude of the low-line voltage  $V_{imL}$  (e.g.,  $V_{Bmin} =$

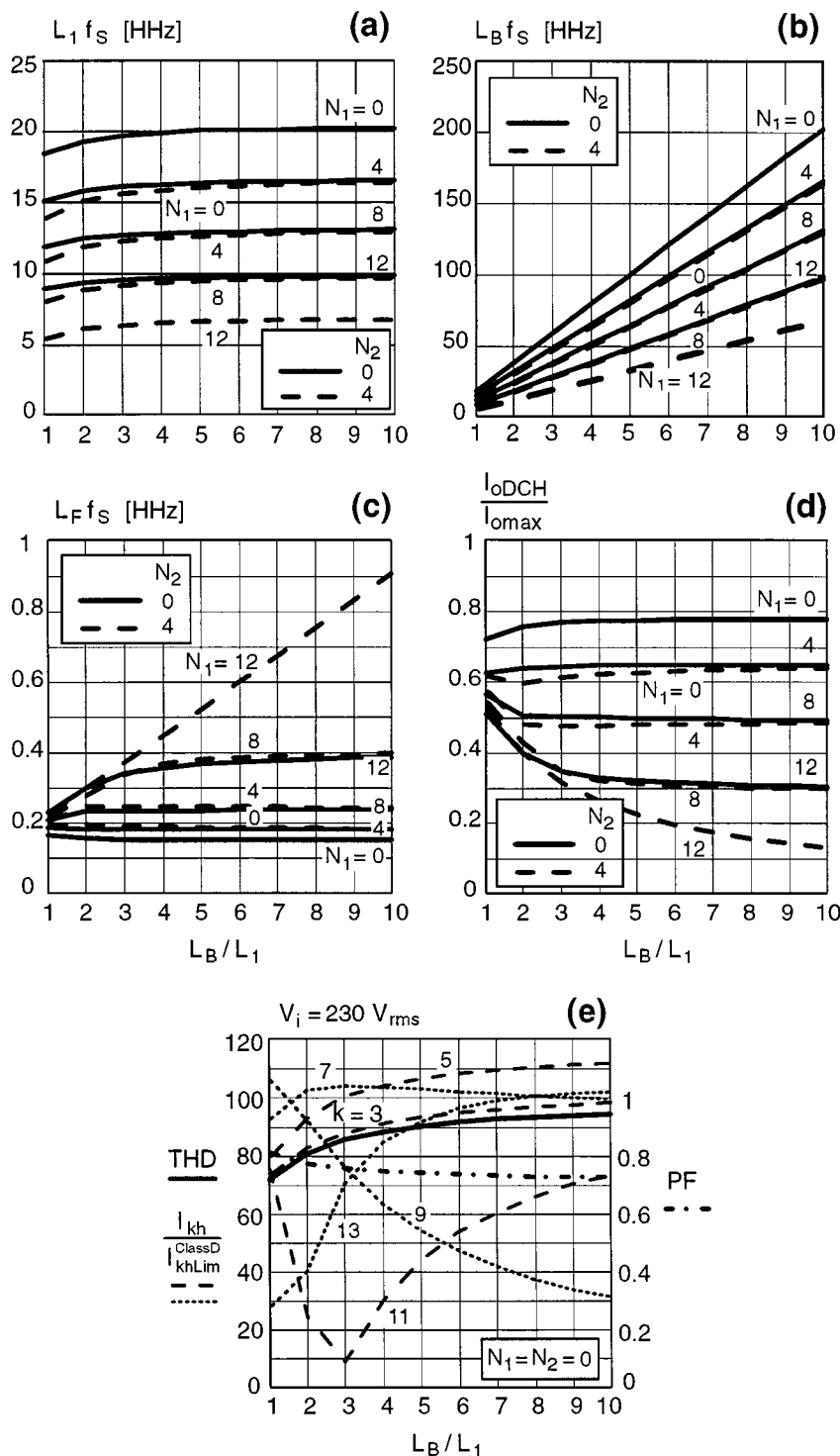


Fig. 8. Design curves for CCM operation of boost inductor ( $V_o = 5 V$ ,  $I_{o max} = 20 A$ ,  $N_S = 3$ ,  $N_P = N_R = 32$ ).

$V_{imL} + 1$ ). Also,  $V_{B min}$  has to satisfy the condition for CCM operation of  $L_B$ , defined in (35).

Writing  $I_o = I_{o max}$  in (54) and substituting (1), (7), (14), (15), (42)–(45), and (47)–(51) into (54) at low line [ $v_{in} = V_{imL} \sin(\omega L t)$ ] and  $V_B = V_{B min}$ , the input–output power balance yields

$$\frac{K_{L_B L}}{L_B f_S} + \frac{K_{L_1 L}}{L_1 f_S} = \frac{V_o I_{o max}}{\eta_L}. \quad (56)$$

Using (56), for a selected ratio of inductances,  $L_1/L_B$ , the product of inductance  $L_1$  and switching frequency  $f_S$  is obtained as

$$L_1 f_S = \eta_L \frac{K_{L_1 L} + \frac{L_1}{L_B} K_{L_B L}}{V_o I_{o max}}. \quad (57)$$

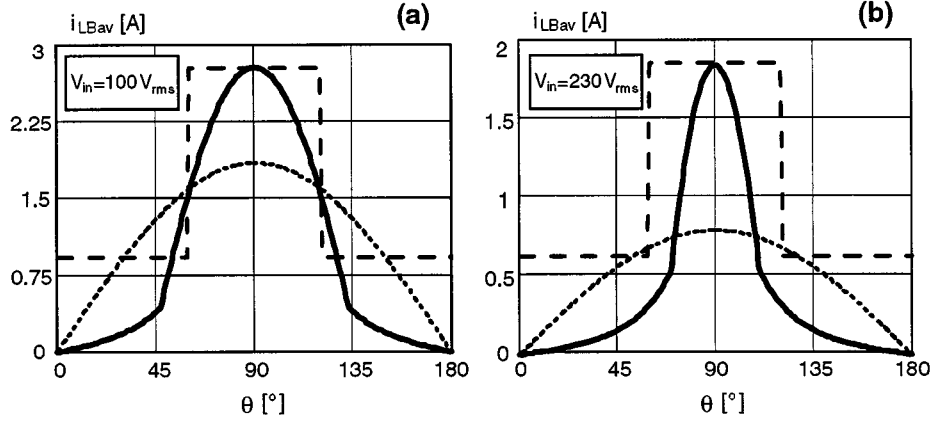


Fig. 9. Line current waveforms in CCM operation of boost inductor ( $V_o = 5$  V,  $I_o = 20$  A,  $N_S = 3$ ,  $N_P = N_R = 32$ ,  $N_1 = N_2 = 0$ ,  $L_B/L_1 = 1.54$ ,  $L_B f_S = 29.31$ ,  $L_1 f_S = 19.05$ ,  $L_F f_S = 0.159$ ; e.g.,  $f_S = 75$  kHz,  $L_B = 391$   $\mu$ H,  $L_1 = 254$   $\mu$ H,  $L_F = 2.11$   $\mu$ H).

Furthermore, substituting (20), (21), and (57) into (55), the product of forward inductance  $L_F$  and switching frequency  $f_S$  is obtained as

$$L_F f_S = \frac{\eta_L}{2\eta_H} \frac{K_{L1L} + \frac{L_1}{L_B} K_{LBL}}{K_{L1H} + \frac{L_1}{L_B} K_{LBH}} \cdot \frac{V_o + V_F}{I_{o\max}} \left(1 - \frac{N_P V_o + V_F}{N_S V_{B\max}}\right). \quad (58)$$

From (57) and (58), for selected values of  $N_P$ ,  $N_R$ ,  $N_S$ ,  $N_1$ , and  $N_2$ , and for selected switching frequency  $f_S$ , inductances  $L_1$ ,  $L_B$ , and  $L_F$  will be determined. The values of  $N_P$ ,  $N_R$ , and  $N_S$  should be selected as for the conventional dc-dc forward converter. Finally,  $N_1$  and  $N_2$ , should be selected according to the following considerations.

Applying the condition for CCM operation of  $L_B$  at high line, from (35) the maximum value of  $N_1 + N_2$  can be obtained as

$$\frac{N_1 + N_2}{N_P} + \frac{L_1 N_2}{L_B N_P} < 1 - \frac{1 + \frac{L_1}{L_B} (1 - D_{\min})}{D_{\min}} \left(1 - \frac{V_{imH}}{V_{B\max}}\right). \quad (59)$$

The minimum value of  $N_1 + N_2$  is zero. In fact, it follows from (33) and (34) that the CCM operation of  $L_B$  best corresponds to the conventional CCM boost ICS at  $N_1 = 0$  and  $N_2 = 0$ . Therefore, the selection of  $N_1$  and  $N_2$  should follow the tradeoff between circuit efficiency and line current distortion.

### C. Design Example

As in Section II, the design procedure is illustrated on the example of a 5-V/20-A universal line-voltage range (90–264 V<sub>rms</sub>) S4ICS forward converter. Maximum bulk-capacitor voltage  $V_{B\max} = 400$  V was specified.

As in Section II,  $N_S = 3$ ,  $N_P = N_R = 32$  are selected. Furthermore,  $V_{B\min} = 130$  V is chosen, which yields  $D_{\max} = 0.455$ . According to (59),  $N_1 + N_2 \leq 17$  at  $L_1 \ll L_B$ , and  $N_1 + 2N_2 \leq 5$  at  $L_1 = L_B$ . Cases when  $L_1 > L_B$

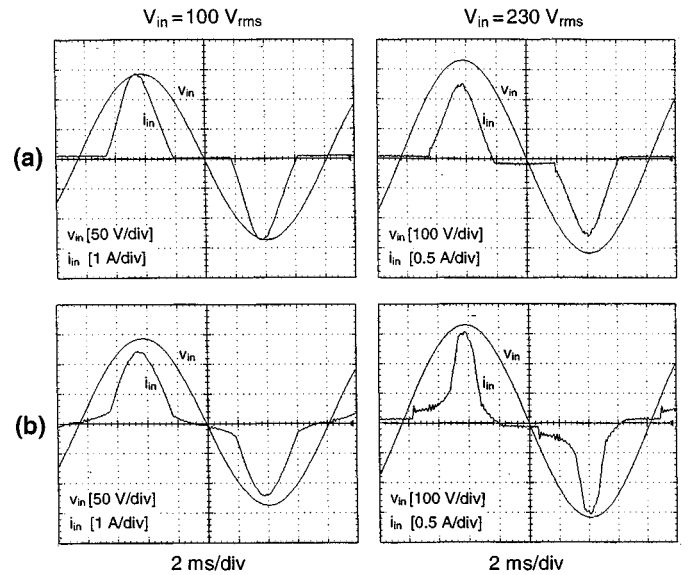


Fig. 10. Experimental line voltage and current waveforms at: (a) DCM and (b) CCM implementation of  $L_B$  ( $V_o = 5$  V,  $I_o = 20$  A).

are of less practical interest because they result in significantly reduced efficiency of the converter. For the selected values of  $N_S$ ,  $N_P$ , and  $N_R$ , design curves are shown in Fig. 8. As can be seen, with increasing  $N_1$  and increasing  $N_2$  the products  $L_1 f_S$  and  $L_B f_S$  are decreasing and the product  $L_F f_S$  is increasing. (Equivalently, with increasing  $L_F f_S$ , the ratio  $I_{oDCH}/I_{o\max}$  is decreasing, which means that  $L_F$  operates in CCM in a wider range of the output current.) It should be also noticed that product  $L_1 f_S$  only slightly depends on the ratio of inductances  $L_B/L_1$ , Fig. 8(a), and, therefore, product  $L_B f_S$  linearly increases with  $L_B/L_1$ , as shown in Fig. 8(b). According to (33) and (34), as  $N_1$  and  $N_2$  increase, the line current becomes more distorted. It will be shown that unlike in the case of the DCM operation of  $L_B$ , where the line current waveforms at nominal high and low lines are almost identical, in the case of the CCM operation of  $L_B$ , the line current at high line is significantly more distorted than at low line. THD of the

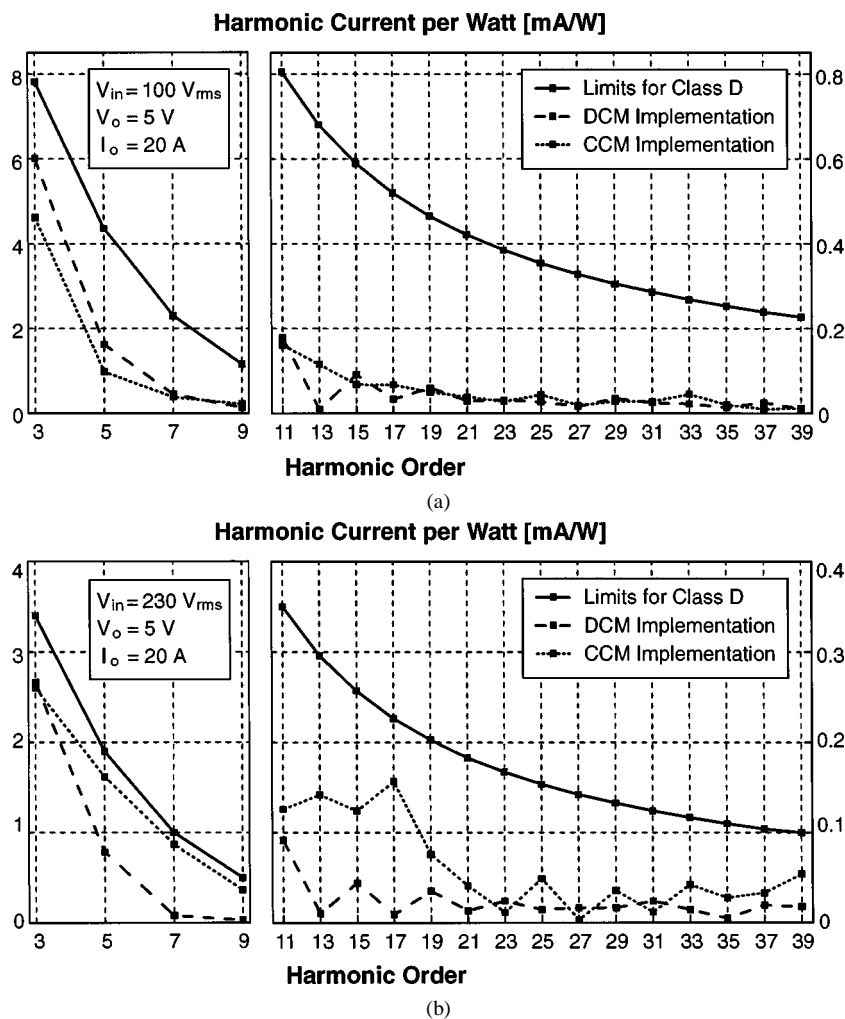


Fig. 11. Experimental line current harmonics at full load at: (a)  $V_i = 100 \text{ V}_{\text{rms}}$  and (b)  $V_i = 230 \text{ V}_{\text{rms}}$ .

line current, input power factor (PF), and the first six odd harmonics of the line current related to the IEC 1000-3-2 Class-D limits [12] versus the ratio of inductances  $L_B/L_1$ , at nominal high line,  $V_i = 230 \text{ V}_{\text{rms}}$ , are shown in Fig. 8(e), for  $N_1 = N_2 = 0$  as an example. It follows from Fig. 8(e) that  $L_B/L_1$  should be selected around 1.5 in order to satisfy the line-current-harmonic requirements. Line current waveforms for  $L_B/L_1 = 1.54$  at both nominal low and high lines are shown in Fig. 9. The IEC 1000-3-2 Class-D envelope and the ideal sinusoidal line current waveform are also shown in Fig. 9. As can be seen from Fig. 9, the line current waveform at  $V_i = 230 \text{ V}_{\text{rms}}$  is significantly distorted compared to that at  $V_i = 100 \text{ V}_{\text{rms}}$ . In fact, the line current is distorted at high line because of the narrow CCM range of  $L_B$  (the boundary angle between DCM and CCM operations of  $L_B$  is  $\theta_{bc} = 69.8^\circ$ ). To reduce  $\theta_{bc}$  at high line,  $D_{\text{min}}$  needs to be increased, as follows from (36). Therefore,  $N_R < N_P$  should be selected. However, a larger unbalance between  $N_R$  and  $N_P$  is not desirable because of the increased voltage stress on the switch and the forward diode. Therefore, transformer reset techniques that allow for a larger maximum duty cycle with reasonable stress on the semiconductor components are more suitable for the implementation of the forward S4ICS in CCM at the universal line-voltage range.

#### IV. EXPERIMENTAL RESULTS

To verify the design procedure of the S4ICS forward converter for both DCM and CCM operations of  $L_B$ , a 5-V/20-A universal line-voltage range (90–264  $\text{V}_{\text{rms}}$ ) S4ICS forward converter shown in Fig. 2 was built. The following components were used for the implementation of the circuit with DCM  $L_B$ :  $C_{\text{in}}—1 \mu\text{F}$ ;  $D_1, D_2$ , and  $D_R—\text{BYM26E}$ ;  $D_F$  and  $D_{\text{FW}}—\text{IR 40CPQ045}$ ; SW-IXTK21N100;  $C_B—330 \mu\text{F}/450 \text{ V}$ ;  $L_F—2.1 \mu\text{H}$ ;  $C_F—3 \times 2200 \mu\text{F}$ ;  $L_B—34 \mu\text{H}$ ; and XF-EER35 core with  $N_P = N_R = 32$  turns,  $N_1 = 20$  turns,  $N_2 = 10$  turns, and  $N_S = 3$  turns ( $L_1 \approx 0$  and  $L_2 \approx 0$ ). For the implementation of the circuit with CCM  $L_B$ , except for inductors  $L_B$  and  $L_1$ , and transformer windings  $N_1$  and  $N_2$ , all other components were the same as for the implementation with DCM  $L_B$ . In the implementation with CCM  $L_B$ ,  $L_B—400 \mu\text{H}$ , XF with  $N_1 = N_2 = 0$ , and  $L_1 = 260 \mu\text{H}$  (external inductance) were used. In both implementations, the same low-cost current-mode pulsewidth modulation (PWM) IC controller (UC3845) was used to implement a fast output-voltage feedback control. The switching frequency of both implementations was constant at 75 kHz throughout the entire line voltage and load range.

TABLE I  
MEASURED PF, THD,  $V_B$ , AND  
EFFICIENCY ( $V_o = 5$  V,  $I_o = 20$  A)

$V_{in}$ [V <sub>rms</sub> ]	DCM $L_B$				CCM $L_B$			
	PF	THD	$V_B$ [V]	$\eta$ [%]	PF	THD	$V_B$ [V]	$\eta$ [%]
90	0.845	61.4	130	76.0	0.912	43.5	128	76.6
100	0.845	61.7	145	76.5	0.899	47.1	143	77.1
132	0.841	63.1	194	77.1	0.858	58.2	193	78.0
180	0.840	63.4	266	76.7	0.820	67.7	265	77.7
230	0.838	63.3	340	75.5	0.796	72.6	338	76.4
264	0.836	63.1	390	74.2	0.785	74.1	388	75.4

Experimental line-current waveforms at both nominal low and high lines, and full load, are shown in Fig. 10. For both implementations of  $L_B$ , the experimental waveforms are in good agreement with the theoretical waveforms. The measured line-current harmonics are shown in Fig. 11. As can be seen, the IEC 1000-3-2 specifications are satisfied for both implementations of  $L_B$ . Table I summarizes the power-factor (PF), total-harmonic-distortion (THD), bulk-capacitor-voltage ( $V_B$ ), and efficiency measurements [including in-rush-current limiter and electromagnetic interference (EMI) filter] at full load. The CCM implementation of  $L_B$  yields  $V_{B\max} = 400$  V and  $V_{DS\max} = 800$  V at 10-A load current, while the DCM implementation of  $L_B$  results in slightly larger values:  $V_{B\max} = 410$  V and  $V_{DS\max} = 830$  V at 12-A load current. All the experimental results are in close agreement with the analytical results.

## V. SUMMARY

A complete design-oriented analysis of the single-stage single-switch input-current shaper which combines the boost-like front end with a dc/dc forward converter is presented. Design equations are derived for both the discontinuous and continuous conduction modes of operation of the boost inductor. The design procedure is demonstrated on a 5-V/20-A universal line-voltage range (90–264 V<sub>rms</sub>) converter. The experimental results are in good agreement with the analytical results.

## REFERENCES

- [1] M. Madigan, R. Erickson, and E. Ismail, "Integrated high-quality rectifier-regulators," in *IEEE Power Electronics Specialists Conf. (PESC) Rec.*, June 1992, pp. 1043–1051.
- [2] M. Brković and S. Čuk, "Novel single stage ac-to-dc converters with magnetic amplifiers and high power factor," in *Proc. IEEE Applied Power Electronics Conf. (APEC)*, Mar. 1995, pp. 447–453.
- [3] R. Redl and L. Balogh, "Design considerations for single-stage isolated power-factor-corrected power supplies with fast regulation of the output voltage," in *Proc. IEEE Applied Power Electronics Conf. (APEC)*, Mar. 1995, pp. 454–458.

- [4] H. Watanabe, Y. Kobayashi, Y. Sekine, M. Morikawa, and T. Ishii, "The suppressing harmonic currents, MS (magnetic-switch) power supply," in *Proc. IEEE Int. Telecommunication Energy Conf. (INTELEC)*, Oct. 1995, pp. 783–790.
- [5] F. Tsai, P. Markowski, and E. Whitcomb, "Off-line flyback converter with input harmonic current correction," in *Proc. IEEE Int. Telecommunication Energy Conf. (INTELEC)*, Oct. 1996, pp. 120–124.
- [6] L. Huber and M. M. Jovanović, "Single-stage, single-switch, isolated power supply technique with input-current shaping and fast output voltage regulation for universal input-voltage-range applications," in *Proc. IEEE Applied Power Electronics Conf. (APEC)*, Feb. 1997, pp. 272–280.
- [7] P. Kornetzky, H. Wei, and I. Batarseh, "A novel one-stage power factor correction converter," in *Proc. IEEE Applied Power Electronics Conf. (APEC)*, Feb. 1997, pp. 251–258.
- [8] Y. S. Lee, K. W. Siu, and B. T. Lin, "Novel single-stage isolated power-factor-corrected power supplies with regenerative clamping," in *Proc. IEEE Applied Power Electronics Conf. (APEC)*, Feb. 1997, pp. 259–265.
- [9] J. Qian and F. C. Lee, "A high efficient single stage single switch high power factor ac/dc converter with universal input," in *Proc. IEEE Applied Power Electronics Conf. (APEC)*, Feb. 1997, pp. 281–287.
- [10] J. Sebastian, M. M. Hernando, P. Villegas, J. Diaz, and A. Fontan, "Input current shaper based on the series connection of a voltage source and a loss-free resistor," in *Proc. IEEE Applied Power Electronics Conf. (APEC)*, Feb. 1998, pp. 461–467.
- [11] G. Hua, "Consolidated soft-switching ac/dc converter," U.S. Patent 5790389, Aug. 4 1998.



**Laszlo Huber** (M'86) was born in Novi Sad, Yugoslavia, in 1953. He received the Dipl. Eng. degree from the University of Novi Sad, Novi Sad, the M.S. degree from the University of Niš, Niš, Yugoslavia, and the Ph.D. degree from the University of Novi Sad in 1977, 1983, and 1992, respectively, all in electrical engineering.

From 1977 to 1992, he was an Instructor at the Institute for Power and Electronics, University of Novi Sad. In 1992, he joined the Virginia Power Electronics Center at Virginia Tech, Blacksburg, as a Visiting Professor. From 1993 to 1994, he was a Research Scientist at the Virginia Power Electronics Center. Since 1994, he has been a Project Engineer at the Power Electronics Laboratory, Delta Products Corporation, Research Triangle Park, NC, the Advanced R&D unit of Delta Electronics, Inc., Taiwan, R.O.C., one of the world's largest manufacturers of power supplies. His 22-year experience includes the analysis and design of high-frequency, high-power-density, single-phase and three-phase power processors; modeling, evaluation, and application of high-power semiconductor devices; and modeling, analysis, and design of analog and digital electronics circuits. He has published more than 60 technical papers, holds two U.S. patents, and has one U.S. patent pending.



**Milan M. Jovanović** (S'86–M'89–SM'89) was born in Belgrade, Yugoslavia. He received the Dipl. Ing. degree in electrical engineering from the University of Belgrade, Belgrade.

Presently, he is the Vice President for Research and Development of Delta Products Corporation, Research Triangle Park, NC, the U.S. subsidiary of Delta Electronics, Inc., Taiwan, R.O.C., one of the world's largest manufacturers of power supplies. His current research is focused on power conversion and management issues for portable data-processing equipment, design optimization methods for low-voltage power supplies, distributed power systems, and power-factor-correction techniques.